Available online at www.sciencedirect.com

ScienceDirect

Ceramics International 40 (2014) 1971–1977

CERAMICS INTERNATIONAL

www.elsevier.com/locate/ceramint

Effect of Y^{3+} substitution on structural, electrical and optical properties of $BiFeO_3$ ceramics

Vikash Singh, Subhash Sharma, Pardeep K. Jha, Manoj Kumar, R.K. Dwivedi*

Department of Physics and Materials Science and Engineering, Jaypee Institute of Information Technology, Noida 201307, India

Received 9 May 2013; received in revised form 27 June 2013; accepted 14 July 2013
Available online 27 July 2013

Abstract

$Bi_{1-x}Y_xFeO_3$ ceramics with compositions $x=0.00$, 0.05, 0.10, 0.15 and 0.20 were synthesized by the solid state reaction route. All the compositions have shown single phase formation with minor impurities. Microstructural studies reveal that Y^{3+} substitution influences grain growth, which in turn affects the dielectric and optical properties of these materials. Dielectric anomalies in temperature dependent dielectric plots at around the magnetic transition temperature (T_N) indicate magneto-electric coupling. Ac conductivity has been found to decrease with increasing Y^{3+} concentration. FTIR spectra show two broad absorption bands due to the overlapping of Fe-O and Bi-O group′s vibrations in the region 400–700 cm^{-1}. The photoluminescence spectra of these ceramics exhibit band edge emission at 458 nm (2.67 eV) in blue region. The emission in green region may be attributed to the transitions related to the defects and Y^{3+} ions.

Keywords: X-ray diffraction; Dielectric and optical properties

1. Introduction

Present soar of interest in multiferroics is due to coexistence of ferroelectric, antiferromagnetic and/or ferroelastic ordering simultaneously at room temperature. Existence of these two polar orders are expected to provide potential for technological applications and understanding of the inherent new physics underlying multiferroic behavior [1,2]. $BiFeO_3$ (BFO) is one of the most investigated multiferroics in which lone pair electrons of Bi^{3+} are responsible for ferroelectricity, and partially filled d orbitals of Fe^{3+} ion contribute to the magnetic ordering in bismuth ferrite [2]. $BiFeO_3$ possesses magnetic order of anti-ferromagnetic (AFM) type below Neel temperature (T_N) ~640 K and ferroelectric order below Curie temperature (T_C) ~1103 K [3–5]. The crystal structure of the $BiFeO_3$ has been reported to be distorted rhombohedral with R3c space group symmetry, which allows anti-phase octahedral tilting and ionic displacements from the centrosymmetric position. The R3c symmetry has permitted the existence of weak ferromagnetic moments, because a cycloid type spatial spin modulation superimposed to the G-type antiferromagnetic spin order, prevents the observation of net magnetization [6,7].

The possibility to suppress the spin modulation with a partial A-site ionic substitution has motivated numerous studies of $Bi_{1-x}A_xFeO_3$ compounds where the substituting elements are rare earth elements. These substitutions are expected to influence the properties and offer the way for elucidating of the powerful mechanism of the ferroelectricity and it is coupling to the magnetic order in multiferroics [8–11]. In view of the above, the substitution of a non rare earth Y^{3+} ion (ionic radius~0.90 Å) in place of Bi^{3+} ion (ionic radius ~1.03 Å) could be explored as one of the worthful studies on structural, electrical and optical properties in multiferroics. In the present paper, we have synthesized $Bi_{1-x}Y_xFeO_3$ ceramics with $x\leq0.20$ by the solid state reaction method. A systematic study of the effect of Y^{3+} doping on the structure, dielectric and optical properties of $BiFeO_3$ has been reported.

2. Experimental details

$Bi_{1-x}Y_xFeO_3$ ceramics with x=0.00, 0.05, 0.10, 0.15 and 0.20 were synthesized by the solid state reaction method. High purity powders of bismuth oxide (Bi_2O_3 ~99.99%, Aldrich),

*Corresponding author. Tel.: +91 120 2594366; fax: +91 120 2400986.
E-mail addresses: rk.dwivedi@jiit.ac.in, rkdwivedi.jiit@gmail.com (R.K. Dwivedi).

0272-8842/$ - see front matter © 2013 Elsevier Ltd and Techna Group S.r.l. All rights reserved.
http://dx.doi.org/10.1016/j.ceramint.2013.07.106

iron oxide (Fe_2O_3 ~99.99%, Aldrich) and yttrium oxide (Y_2O_3 ~99.99%, Aldrich) were used as starting materials. In order to obtain phase-pure and dense samples, appropriate sintering temperatures were carefully selected from 820–830 °C for 2 h with varying amounts of Y^{3+} substitutions. X-ray diffraction (XRD) patterns of sintered samples were recorded at room temperature using an X-ray Powder Diffractometer (Bruker D8 Advance) with Cu Kα radiation (1.5418 Å). Microstructure of the synthesized samples has been studied using scanning electron microscope (SEM) and the average grain size has been determined using line intercept method. For this, it is necessary to count the number of grains intersected by each of these line segments. Average line length intersection is calculated according to the following relation:

$$\text{ave. line length intersection} = \frac{\text{length of the line drawn on SEM image}}{\text{ave. no. of grain boundary intersections}}$$

Average grain size 'd' can be obtained using the formula as given below:

$$d = \frac{\text{ave. line length intersected}}{\text{magnification}}$$

Dielectric measurements from room temperature to 550 °C at deferent frequencies were carried out using an automated LCR Meter (HIOKI 3532-50 Hi Tester). Room temperature photoluminescence emission spectra were recorded by Perkin Elmer LS55. Fourier transformed infrared spectroscopy (FTIR) was employed to study various vibrational bands in Y^{3+} ions substituted BFO ceramics using Perkin Elmer BXII spectrometer.

3. Results and discussion

Fig. 1 (a) shows room temperature XRD patterns of $Bi_{1-x}Y_xFeO_3$ (BYFO) system with x=0.00, 0.05, 0.10, 0.15 and 0.20. Few impurity peaks of $Bi_2Fe_4O_9$ and $Bi_{36}Fe_2O_{57}$ have been observed in all the compositions [9]. All the peaks in the XRD patterns of these samples have been indexed according to the crystal structure of pure $BiFeO_3$ and lattice parameters have been determined. The unit cell volume has been found to be decreased with x (see Table 1). The calculated values of lattice parameters indicate that there is a continuous change of lattice constant as a result of replacing the Bi^{3+} ion with the Y^{3+} ion. The decrease in the lattice volume may be attributed to the substitution of smaller Y^{3+} ions (0.90 Å) in place of Bi^{3+} ions (1.03 Å) in the matrix of BFO lattice. Variation of lattice parameters with composition is shown in Fig. 1(b).

Williamson-Hall proposed diffraction line broadening due to crystallite size and strain contribution as a function of diffraction angle which can be written in the form of mathematical expression $\beta_{hkl}=\beta_t+\beta_\varepsilon$ where β_t is due to crystallite size contribution, β_ε is due to strain induced broadening and β_{hkl} is the full-width at half of the maximum intensity (FWHM) of instrumental corrected broadening [12]. Crystallite size contribution is calculated using the Scherer formula $\beta_t = k\lambda/t\cos\theta$, where k is the shape factor; λ is the wavelength of the x-ray used. Strain contribution is calculated by $\beta_\varepsilon = 4\varepsilon\tan\theta$, where ε is the micro-strain. It is clear that line broadening is a combination of crystallite size and strain, which is represented by the equation:

$$\beta_{hkl} = \frac{k\lambda}{t\cos\theta} + 4\varepsilon\tan\theta$$

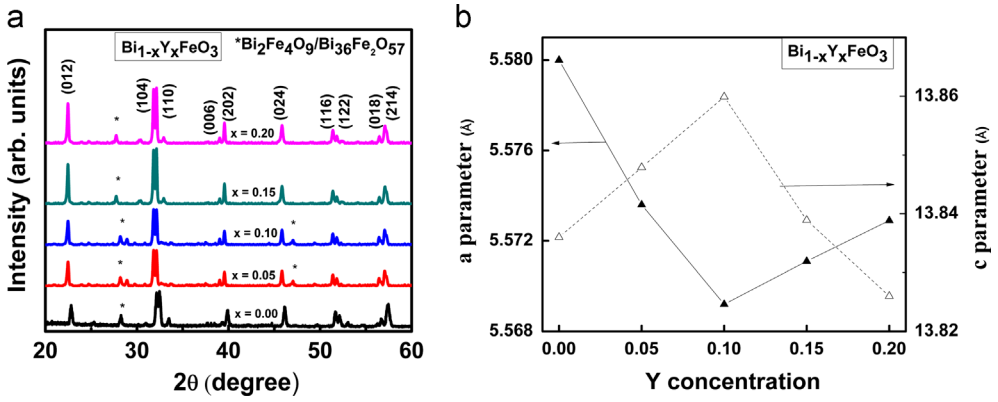

Fig. 1. (a) X-ray diffraction patterns of $Bi_{1-x}Y_xFeO_3$ (x≤0.20) powders and (b) variation of lattice parameters with Y concentration.

Table 1
Lattice parameter, volume and average grain size of compositions with x≤0.20 in the system $Bi_{1-x}Y_xFeO_3$.

Concentration x in $Bi_{1-x}Y_xFeO_3$	a (Å)	c (Å)	Volume (Å)^3	Average grain size (μm)
0.00	5.580	13.836	373.07	–
0.05	5.5736	13.8479	372.54	4
0.10	5.5692	13.8599	372.62	2
0.15	5.5711	13.8389	372.06	2
0.20	5.5729	13.826	371.52	1

This is further simplified as

$$\beta_{hkl}\cos\theta_{hkl} = \frac{k\lambda}{t} + 4\varepsilon\ \sin\theta_{hkl}$$

Value of $\beta_{hkl}\cos\theta_{hkl}$ as a function of $4\varepsilon\sin\theta_{hkl}$ is plotted (shown in Fig. 2a) and ε is calculated through the linear fit (shown in Fig. 2b). This model is known as the uniform deformation model [13]. Crystallite size and strain both decrease with increasing Y^{3+} concentration, which may be due to smaller size of Y^{3+} ion.

Fig. 3 shows scanning electron micrographs of $Bi_{1-x}Y_xFeO_3$ (x=0.05, 0.10, 0.15 and 0.20) ceramics. It has been observed that the microstructure of Y^{3+} doped BFO samples is dense. With increasing Y^{3+} concentration, the crystallization becomes poor and hence, precise determination of grain size is difficult. However, the average grain size, determined from

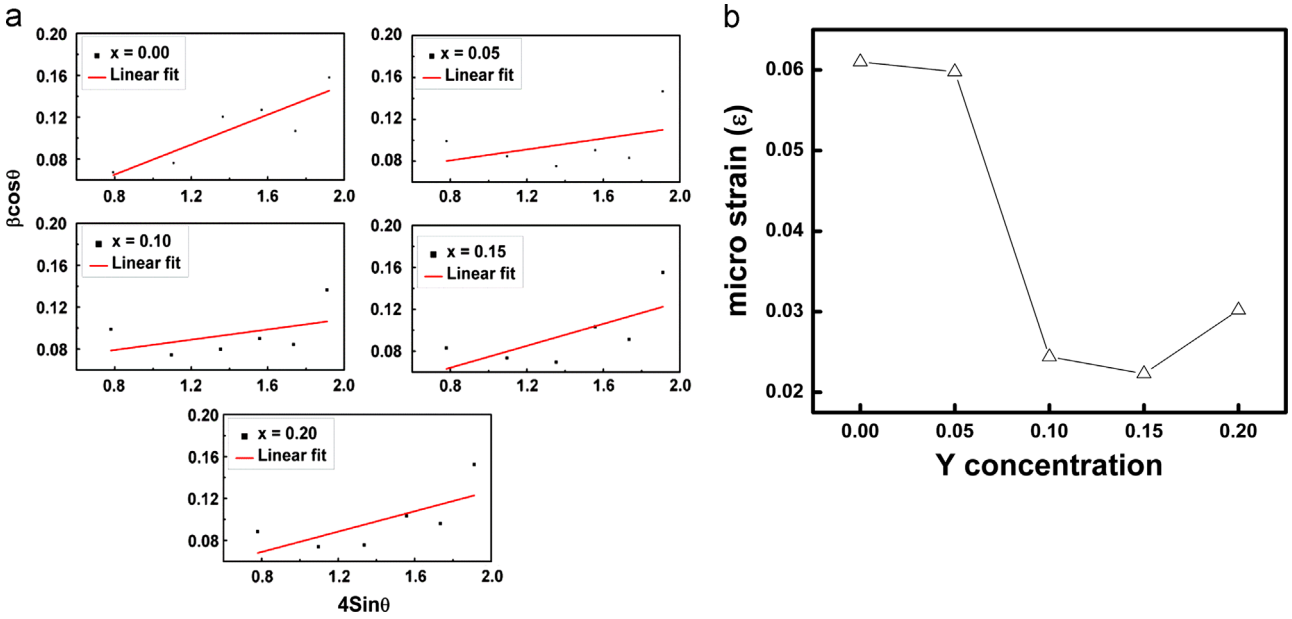

Fig. 2. (a) The *W–H* analysis plots of pure and doped $BiFeO_3$ and (b) variation of strain with Y^{3+} concentration.

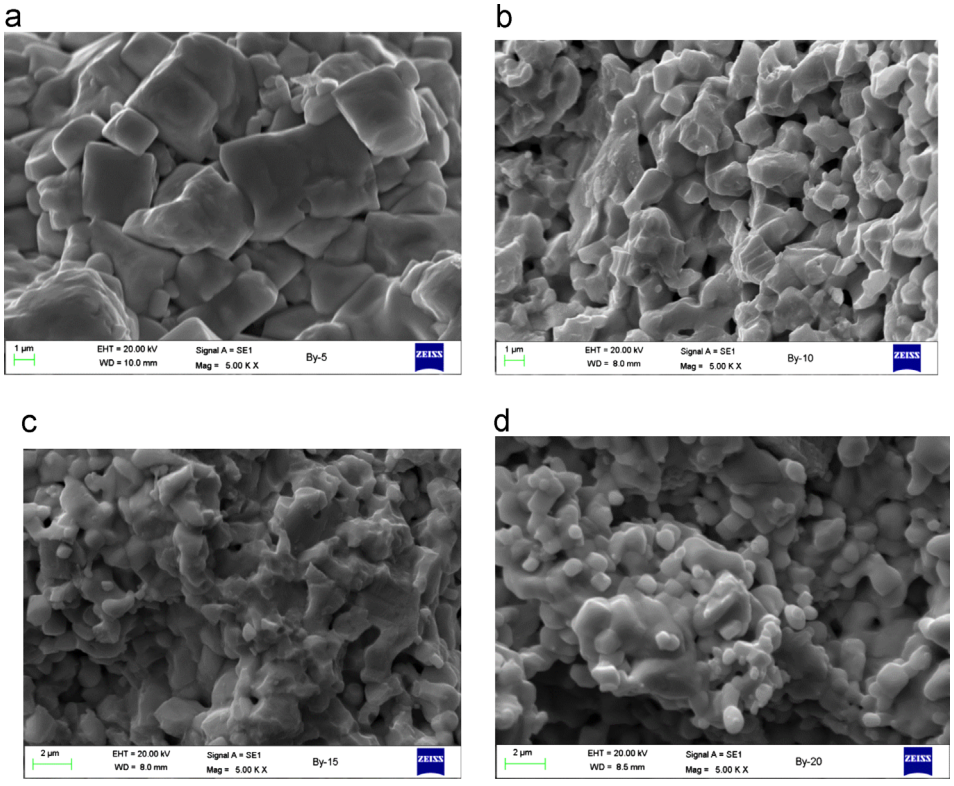

Fig. 3. SEM micrographs of $Bi_{1-x}Y_xFeO_3$ ceramics for compositions (a) 0.05 (b) 0.10 (c) 0.15 and (d) 0.20.

line intercept method is given in the Table 1, which has been found to decrease with x. Average grain size in all the samples is less than 4 μm and almost spherical grains are observed for the sample with $x=0.20$.

Variation of relative dielectric constant (ε_r) for compositions with $x\leq0.20$ in $Bi_{1-x}Y_xFeO_3$ system as a function of frequency is shown in Fig. 4. It shows that with increasing Y^{3+} concentration, the dielectric constant increases for $0<x\leq0.20$, however less than pure BFO. The value of the dielectric constant is high at low frequencies and decreases with increasing frequency. Loss tangent factor (tan δ) is also found to decrease with increasing x. It is clear from ε_r vs log f plot for $x>0.05$ that dielectric constant remains frequency independent up to a certain frequency. This behavior can be understood in terms of space charge relaxation. At low frequencies, the space charges are able to follow the frequency of the applied field but at high frequencies, space charge may not have enough time to build up and get relaxed out. Dielectric loss follows the same trend as the dielectric constant over the whole frequency range from 10 kHz to 1 MHz.

Fig. 5 shows the temperature dependence of the dielectric constant (ε_r) and tan δ of Y^{3+} doped BFO samples at 100 kHz for compositions with $x\leq0.20$. Replacement of Bi^{+3} ions by Y^{3+} ions ($x=0.05$–0.10) modifies the dielectric characteristics of BFO, resulting in vanishing of the anomaly and substantial

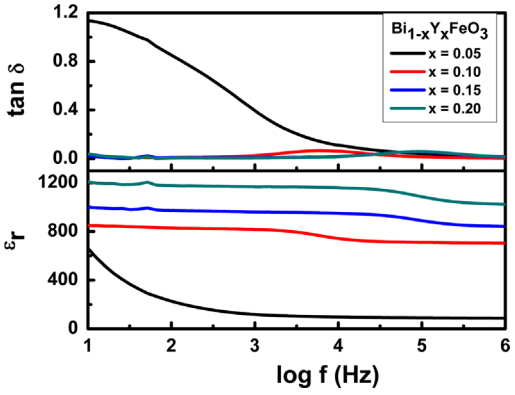

Fig. 4. Frequency dependence of dielectric constant and dielectric loss at room temperature for $x\leq0.20$ in $Bi_{1-x}Y_xFeO_3$ ceramics.

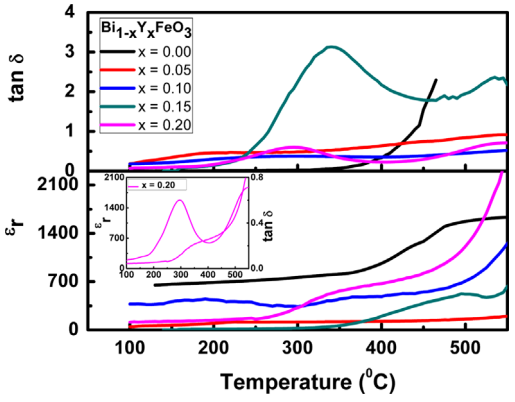

Fig. 5. Temperature dependence of dielectric constant and dielectric loss at 100 kHz for $x\leq0.20$ in $Bi_{1-x}Y_xFeO_3$ ceramics.

reduction of tan δ. The replacement of some volatile Bi^{3+} ions with non-volatile Y^{3+} ions may avoid creation of oxygen ion vacancies causing stabilization of the Fe^{3+}/Fe^{2+} coupled oxygen vacancy interaction [14,15]. Dielectric anomalies are observed in dielectric constant vs temperature plots at 376 °C and 318 °C for $x=0.15$ and 0.20, respectively. Broad peaks are observed in loss tangent vs temperature plots at slightly different temperatures i.e. 340 °C and 289 °C for $x=0.15$ and 0.20, respectively (see Fig. 5). The dielectric anomaly in ε_r vs T plots in all the compositions is observed near the magnetic transition temperature T_N, which is the typical AFM characteristic temperature of BFO. This type of dielectric anomaly in magneto-electrically ordered systems was predicted by the Landau-Devonshire theory of phase transition as an influence of vanishing magnetic order on the electric order [16]. Also for $x=0.20$ sample, permittivity is much higher and loss is very low as compared to the other compositions in the entire range of temperature, indicating the reduced oxygen vacancy concentration with increasing Y^{3+} doping. A sudden jump in the dielectric constant at around 450 °C is observed which slightly varies from one sample to another sample, can be clearly seen in the inset of Fig. 5 for $x=0.20$. This sudden jump could be attributed to a space charge contribution (Maxwell–Wagner polarization) which can be seen as a loss peak in tan δ vs T plots. These observations are in accordance to the recent report by Kamba et al. [17]. Maxwell–Wagner polarization in our samples may be due to the local charge imbalance caused by the oxygen non-stoichiometry. Further shift in the dielectric anomaly from 376 °C to 318 °C may be attributed to Y^{3+} substitution as Yttrium based multiferroic ($YMnO_3$) exhibits T_N at ~40 K [18].

In Fig. 6, shows the variation of conductivity with temperature of Y^{3+} doped BFO samples for $x\leq0.20$. Conductivity showed a gradual increase with increasing temperature. The activation energy values (E_A) are calculated using the Arrhenius equation $\sigma_{ac}=\sigma_0\exp(-E_A/kT)$ in three linear region with different slopes. The conductivity in these temperature regimes can be explained on the basis of different activation energy values. It is possible to link each region to the movements of electrical charges which are thermally activated. In the first temperatures regime up to 200 °C, the

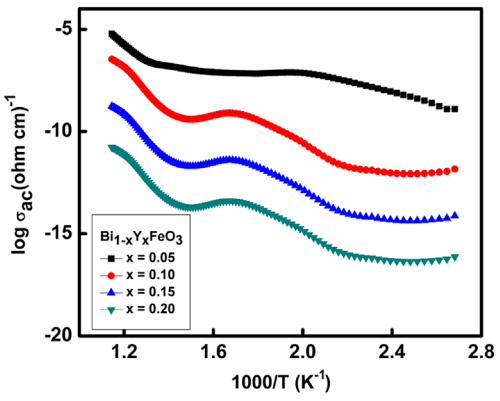

Fig. 6. Variation of log σ_{ac} with inverse of temperature for the compositions with $x\leq0.20$ in $Bi_{1-x}Y_xFeO_3$ ceramics.

activation energy is as low as 0.07 eV which may be attributed to the local electron transport due to the hoping at the neighboring sites [19,20]. The existence of conduction electrons is due to the deficiency of oxygen in BFO. In the second region from 220 °C to 350 °C, the activation energy is 0.4 eV, about five times the activation energy in the region one. This value of activation energy may be attributed to the singly ionized oxygen vacancies movements. In the third region above 400 °C, the activation energy is 0.8 eV, which is two times the value observed in the second region. This kind of activation energy actually corresponds to the doubly ionized oxygen vacancy motion from one site to the other [21,22]. As the temperature increases, impurity conduction ceases and electrical conduction, attributed to the doubly ionized oxygen vacancies, sets on according to the following reaction [22]:

$$O_0 \rightarrow \left(\frac{1}{2}\right)O_2 + V_0'' + 2e'$$

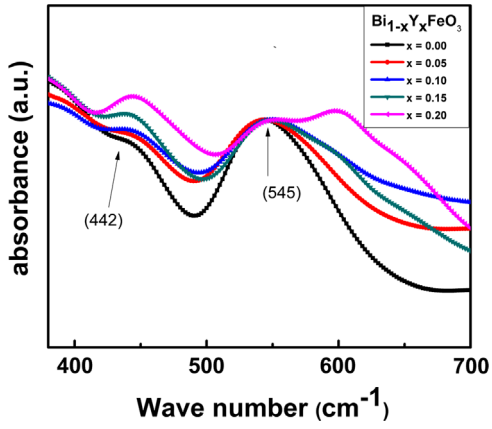

Fig. 7. Room temperature IR absorption spectra of compositions with $x \leq 0.20$ in $Bi_{1-x}Y_xFeO_3$ ceramics.

Room temperature FTIR absorption spectra of Y^{3+} ions doped BFO ceramics are shown in Fig. 7. The IR spectra gives information about the chemical and molecular structure changes in BFO due to the changes in Fe-O bond during sintering as well as when foreign atoms are doped in BFO. Two broad absorption bands are observed near 545 and 442 cm^{-1} due to the overlapping of Fe-O and Bi-O groups' vibrations. The broad band near 545 cm^{-1} is attributed to Fe-O and Bi-O stretching in BiO_6 and FeO_6 octahedra [23,24], second broad band absorption peak near 442 cm^{-1} is attributed to bending of Fe-O and Bi-O groups. Shift of the absorption peaks around 442 cm^{-1} to higher wave number side is clearly observed with increasing Y^{3+} concentration. This indicates that bending of Fe-O and Bi-O bonds increases with composition x, suggesting the deformation in the FeO_6 octahedra increases with Y^{3+} concentration in these samples [11].

Photoluminescence (PL) spectra of pure and Y^{3+} doped BFO samples at room temperature are shown in Fig. 8. PL excitation (at 440 nm) for pure BFO resulted in an intense blue emission, which is clearly visible. The spectrum shows a strong emission line at 458 nm in the blue region along with a weak hump at 508 nm. We assign this dominant emission at 458 nm as a band to band transition in BFO corresponding to the band gap of 2.67 eV [25]. Any other emission of lower energies must come from various impurities or defect levels

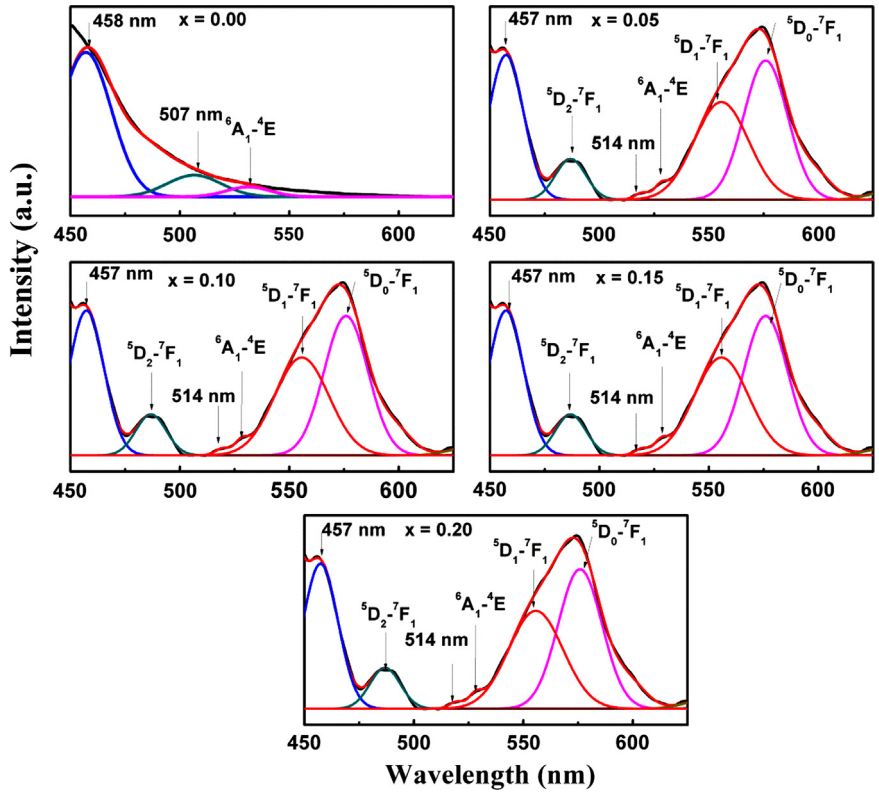

Fig. 8. Room temperature PL spectra of compositions with x in $Bi_{1-x}Y_xFeO_3$ ceramics.

inside the band gap. The weak hump around 508 nm may be ascribed to oxygen vacancy defects present in the sample [26]. The weak yellow emission at around 540 nm for all the samples may be due to the electronic transition of Bi^{3+} between $^6A_1$ and ^4E. For all Y^{3+} doped BFO samples, we observed strong blue emission around 457 nm and weak secondary emissions at around 488 nm followed by a broad yellow emission. The weak secondary emission at around 488 nm for all Y^{3+} doped BFO samples may be attributed to the transition of Y^{3+} between $^5D_2$ and $^7F_1$ states [27,28]. The weak hump at around 514 nm may be due to oxygen vacancy defects present in Y^{3+} doped BFO samples. The intensity of the peaks corresponding to oxygen vacancies and Bi^{3+} transition is reduced and oxygen vacancies transition shifted from 508 nm (x=0.00) to 514 nm (x=0.20) with increasing Y^{3+} concentration. The broad yellow emission, observed in all Y^{3+} doped BFO samples, is due to the overlapping of different transitions of Y^{3+} ions. After deconvolution, two peaks can be identified at 561 and 584 nm. The intensity of broad yellow emission increases with increasing Y^{3+} concentrations in BFO. These weak yellow emissions may be ascribed to the electronic transitions of Y^{3+} between $^5D_1$ and $^7F_1$ (561 nm) and $^5D_0$ and $^7F_1$ (584 nm) states [28]. These blue and yellow emissions in visible region for Y^{3+} doped BFO samples may find potential applications in optoelectronic devices.

4. Conclusions

$Bi_{1-x}Y_xFeO_3$ ceramics with compositions x=0.05, 0.10, 0.15 and 0.20 have shown single phase formation with minor impurities. Dielectric anomaly at low temperature may be ascribed to the magnetic transition in BFO and second dielectric peak at ~450 °C may be attributed to the Maxwell–Wagner type polarization. Decrease in conductivity with x may be attributed to the suppression of defects in these ceramics which is also supported by decrease in dielectric loss. The average grain size in all the samples is found to be less than ~4 μm. The presence of two vibrational modes at 442 cm^{-1} and 545 cm^{-1} in the FTIR spectra may correspond to the bending and stretching of Bi-O and Fe-O bonds respectively. Shift of absorbance peak at 442 cm^{-1} with x may be attributed to the distortion in FeO_6 octahedra. PL spectra of compositions with $x \leq 0.20$ show blue emission at 458 nm, indicating the optical band gap of 2.67 eV. The emissions at 561 and 584 nm in yellow region may be attributed to the electronic transitions of Y^{3+} states. The optical band gap in the blue region along with yellow emissions may find applications in optoelectronic devices.

Acknowledgment

Author R.K. Dwivedi is thankful to the Department of Science and Technology (DST) and Defense Research and Development Organisation (DRDO), Govt. of India, New Delhi for financial support. One of the authors, Vikash Singh is also thankful to Jaypee Institute of Information Technology for Teaching Assistanceship.

References

[1] R. Ramesh, N.A. Spaldin, Multiferroics: progress and prospects in thin films, Nature Materials 6 (2007) 21.
[2] S.W. Cheong, M. Mostovoy, Multiferroics: a magnetic twist for ferroelectricity, Nature Materials 6 (2007) 13.
[3] W. Eerenstein, N.D. Mathur, J.F. Scott, Multiferroic and magnetoelectric materials, Nature (London) 442 (2006) 759.
[4] W. Kaczmarek, Z. Pajak, Differential thermal analysis of phase transitions in $(Bi_{1-x}La_x)FeO_3$ solid solution, Solid State Communications 17 (1975) 807.
[5] I. Sosnowaska, T. Peterlin-Neumaier, E. Steichele, Spiral magnetic ordering in bismuth ferrite, Journal of Physics C 15 (1982) 4835.
[6] C. Ederer, N.A. Spaldin, Weak ferromagnetism and magnetoelectric coupling in bismuth ferrite, Physical Review B 71 (2005) 060401.
[7] J.R. Cheng, N. Li, L.E. Cross, Structural and dielectric properties of Ga-modified$BiFeO_3$–$PbTiO_3$ crystalline solutions, Journal of Applied Physics 94 (2003) 5153.
[8] A.B. Souchkov, J.R. Simpson, M. Quijada, H. Ishibashi, N. Hur, J.S. Ahn, S.W. Cheong, A.J. Millis, H.D. Drew, Exchange interaction effects on the optical properties of $LuMnO_3$, Physical Review Letters 91 (2003) 027203.
[9] A.P. Litvinchuk, M.N. Iliev, V.N. Popov, M.M. Gospodinov, Raman and infrared-active phonons in hexagonal $HoMnO_3$ single crystals: magnetic ordering effects, Journal of Physics: Condensed Matter 16 (2004) 809.
[10] V. Singh, S. Sharma, R.K. Dwivedi, M. Kumar, R.K. Kotnala, N.C. Mehra, R.P. Tondon, Structural, dielectric, ferroelectric and magnetic properties of $Bi_{0.80}A_{0.20}FeO_3$ (A=Pr,Y) multiferroics, Journal of Superconductivity and Novel Magnetism 26 (2013) 657.
[11] V. Singh, S. Sharma, R.K. Dwivedi, M. Kumar and R.K. Kotnala, Multiferroic and optical properties of Pr-substituted bismuth ferrite ceramics, Physica Status Solidi A 210 (7), 2013, 1442.
[12] Y. Rosenberg, V.S. Machavariani, V. Voronel, S. Garber, A. Rubshtein, AI. Frenkel, Strain energy density in the x-ray powder diffraction from mixed crystals and alloys, Journal of Physics: Condensed Matter 12 (2000) 8081.
[13] V. Biju, N. Sugathan, V. Vrinda, S.L. Salini, Estimation of lattice strain in nanocrystalline silver from X-ray diffraction line broadening, Journal of Materials Science 43 (2008) 1175.
[14] F. Huang, X. Lu, W. Lin, X. Wu, Yi Kan, J Zhu, Effect of Nd dopant on magnetic and electric properties of $BiFeO_3$ thin films prepared by metal organic deposition method, Applied Physics Letters 89 (2006) 242914.
[15] H. Uchida, R. Ueno, H. Funakubo, S. Koda, Crystal structure and ferroelectric properties of rare-earth substituted $BiFeO_3$ thin films, Journal of Applied Physics 100 (2006) 014106.
[16] V.R. Palkar, D.C. Kundaliya, S.K. Malik, S. Bhattacharya, Magnetoelectricity at room temperature in the $Bi_{0.9-x}Tb_xLa_{0.1}FeO_3$ system, Physical Review B 69 (2004) 212102.
[17] S. Kamba, D. Nuzhnyy, M. Savinov, J. Sebek, J. Petzelt, J. Prokleska, R. Haumont, J. Kreisel, Infrared and terahertz studies of polar phonons and magnetodielectric effect in multiferroic $BiFeO_3$ ceramics, Physical Review B 75 (2007) 024403.
[18] H. Fukumura, S. Matsui, H. Harima, K. Kisoda, T. Takahashi, T. Yoshimura, N. Fujimura, Raman scattering studies on multiferroic $YMnO_3$, Journal of Physics: Condensed Matter 19 (2007) 365239.
[19] C. Ang, Z. Yu, L.E. Cross, Oxygen-vacancy-related low-frequency dielectric relaxation and electrical conduction in Bi:$SrTiO_3$, Physical Review B 62 (2000) 228.
[20] S. Saha, S.B. Krupanidhi, Dielectric response and complex impedance spectroscopy studies in pulsed laser ablated (Ba, Sr)TiO_3 thin films, Integrated Ferroelectrics 33 (2001) 331.
[21] W.S. Warren, K. Vanheusden, D. Dimos, G.E. Pike, B.A. Tuttle, Oxygen vacancy motion in perovskite oxides, Journal of the American Ceramic Society 79 (1996) 536.

[22] R.K. Dwivedi, Devendra Kumar, Om Parkash, Valence compensated perovskite system $Ca_{1-x}La_xTi_{1-x}Cr_xO_3$: Part-II; Electrical transport behavior, Journal of Materials Science 36 (2001) 3649.

[23] R.K. Mishra, Dillip K. Pradhan, R.N.P. Choudhary, A. Banerjee, Effect of yttrium on improvement of dielectric properties and magnetic switching behavior in $BiFeO_3$, Journal of Physics: Condensed Matter 20 (2008) 045218.

[24] Subba G.V. Rao, C.N.R. Rao, Infrared and electronic spectra of rare earth perovskites: ortho-chromites, -manganites and -ferrites, Applied Spectroscopy 24 (1970) 436.

[25] F. Gao, Y. Yuan, K.F. Wang, X.Y. Chen, F. Chen, J.M. Liu, Z.F. Ren, Preparation and photoabsorption characterization of $BiFeO_3$ nanowires, Applied Physics Letters 89 (2006) 102506.

[26] K. Vanheusden, C.H. Seager, W.L. Warren, D.R. Tallant, J.A. Vogit, Correlation between photoluminescence and oxygen vacancies in ZnO phosphors, Applied Physics Letters 68 (1996) 403.

[27] S. Mukherjee, V. Sudarsan, R.K. Vatsa, A.K. Tyagi, Luminescence studies on lanthanideions(Eu^{3+}, Dy^{3+} and Tb^{3+}) doped YAG:Ce nanophosphors, Journal of Luminescence 129 (2009) 69.

[28] Mihail Nazarov, Young Jin Kim, Eun Young Lee, Kyoung-In Min, Mun Seok Jeong, Su Woong Lee, Do Young Noh, Luminescence and Raman studies of $YNbO_4$ phosphors doped by Eu^{3+}, Ga^{3+}, and Al^{3+}, Journal of Applied Physics 100 (2010) 014106.